Spectropolarimetry for space object identification

Snel, Ralph ; Mr. Vasilescu, B.V.; Di Iorio, Eugenio Iorio; Piron, P.; Loicq, J.J.D.; Ferrario, Ivan; Silvestri, Fabrizio

Citation (APA)
Snel, R., Mr. Vasilescu, B. V., Di Iorio, E. I., Piron, P., Loicq, J. J. D., Ferrario, I., & Silvestri, F. (2023). Spectropolarimetry for space object identification. In D. L. Hickman, H. Bursing, G. W. Kamerman, & O. Steinvall (Eds.), *Proceedings volume 12737 Spie security + defence | 3-7 September 2023 Electro-optical and infrared systems: technology and applications XX: Technology and Applications XX* (Vol. 12737). Article 127370X (Proceedings of SPIE - The International Society for Optical Engineering; Vol. 12737). SPIE. https://doi.org/10.1117/12.2689038

Important note
To cite this publication, please use the final published version (if applicable).
Please check the document version above.

PROCEEDINGS OF SPIE

Spectropolarimetry for space object identification

Ralph Snel, Bogdan Vasilescu, Eugenio Di Iorio, Pierre Piron, Jérôme Loicq, et al.

Spectropolarimetry for space object identification

Ralph Snel[a], Bogdan Vasilescu[b], Eugenio Di Iorio[a], Pierre Piron[b],
Jérôme Loicq[b], Ivan Ferrario[a], Fabrizio Silvestri[a]

[a]TNO Netherlands Organisation for Applied Scientific Research, Stieltjesweg 1, 2628 CK Delft, the Netherlands; [b]Delft University of Technology, Kluyverweg 1, 2629 HS Delft, the Netherlands

ABSTRACT

A novel method for space object identification is proposed, based on full Stokes spectropolarimetry in the visible and near-infrared wavelength range. Space objects that have been previously detected and are illuminated by the sun can be observed with a telescope to simultaneously obtain intensity, spectra, and polarimetry, and compose light curves of these parameters as function of time. The intention is to thus assign a unique identification, or at least a classification to these objects.

Single, double, and multiple reflections of sunlight off the space object (natural or artificial objects, including debris) will introduce spectrally dependent polarisation into the scattered light, the spectral signature of which is affected by the complex refractive index of the scattering materials and the geometry. The simultaneous measurement of the full Stokes vector allows separation of the light source unpolarised spectral signatures on the one hand from the polarisation spectral features on the other hand.

To illustrate the concept, we have performed a number of simulations for double scattering off a small selection of materials, for a large range of scattering geometries. Examples of individual scattering geometries and statistical summaries of all geometries are presented.

A demonstrator spectropolarimeter is being built, we present an overview of the design and the high level planning, as well as some predicted performance parameters.

Keywords: Spectropolarimetry, polarimetry, space object identification, UV-vis-NIR, scattered sunlight

1. INTRODUCTION

With the ever-increasing number of artificial satellites in orbit around the Earth, space objects may need some kind of identification more than just their orbital elements [1][2]. Spectroscopy [3] and polarimetry [4] can be used to increase the knowledge about previously detected space objects. We propose to combine both approaches and use full Stokes vector spectropolarimetry for space object identification.

This paper present the rationale behind this choice (Section 2), the polarisation modulator chosen (Section 3), the design of a breadboard spectropolarimeter to demonstrate the principle and learn about spectropolarimetric behaviour of materials and satellites (Section 4), the design of a test bench to characterise the polarisation behaviour of the components in the breadboard (Section 5), the plans for data acquisition and analysis (Section 6), and concludes with a summary and discussion (Section 7).

2. SPECTROPOLARIMETRY FOR SPACE OBJECT SIGNATURE DETECTION

Starting with the spectral complex index of refraction of dielectric media and using the Fresnel equations and a scattering or reflecting geometry, the full Stokes vector of the reflected light can be calculated for any wavelength for which the index of refraction is specified, assuming single reflection off the surface, thus excluding volume scattering effects. Also, multiple reflections can be calculated this way. Figure 2-1 shows the result of the calculation of the spectrally resolved normalised Stokes vector for double reflection off two materials, aluminium and silicon, under a scattering geometry of 50 degrees angle of incidence on both the first and second surface, with a 45-degree rotation of the coordinate frame to produce out-of-plane scattering and promote the generation of circular polarisation. Unpolarised illumination was used in this calculation. Note how the Q/I curves overlap or nearly overlap for linear polarisation (Q/I and U/I) and how the differences become more distinct for the circular polarisation component (V/I).
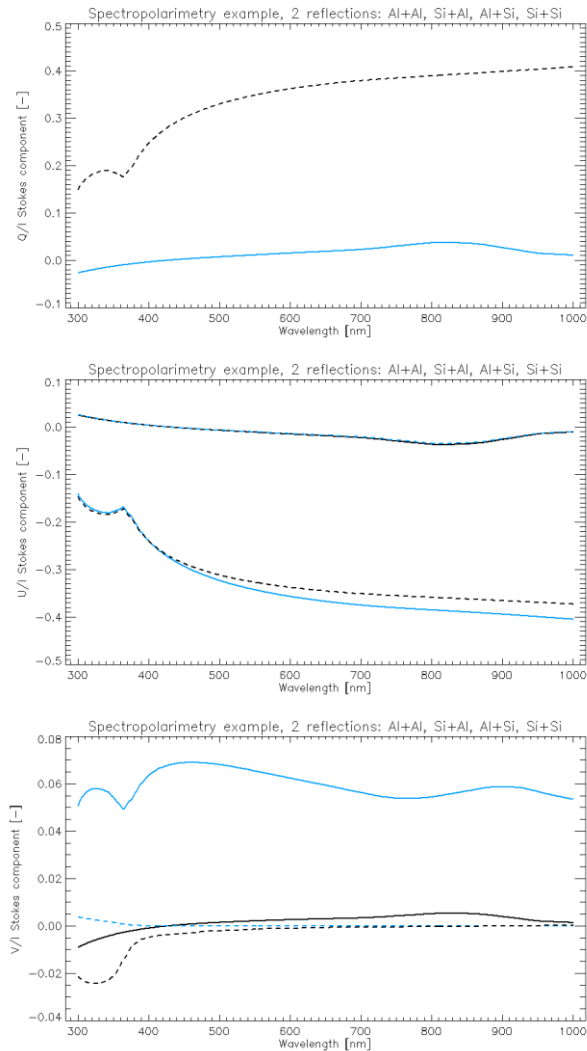
Figure 2-1. Wavelength dependent Stokes vector parameters Q/I (top), U/I (middle), and V/I (bottom) for the geometry and materials described in the text. The full black curve corresponds to two reflections off aluminium, the full blue curve for reflection off aluminium and silicon in that order, the dashed blue curve for silicon and aluminium, and the dashed black curve for two reflections off silicon.

This simple simulation shows that the wavelength dependence of the complex indices of refraction, as well as the order of reflection of the two surfaces, can affect the spectrally resolved Stokes parameters, in particular the circular polarisation component.

In more realistic cases, reflection of sunlight off a satellite will be composed of a mix of single- and multiple scattering, weighed with the relative scattering area and reflectivity for the various light paths from the sun to the observer. Figure 2-2 shows an example of possible light paths in a rendered image of a satellite, note the reflections of the gold-coloured multi-layer insulation (MLI) in the dark solar panels, and the reflections of the solar panels in the MLI. As the illumination and viewing geometry changes over the orbit of a satellite, flares of single- or multiple reflection may arise, carrying potentially distinctive information of the surface materials and configuration of the satellite.
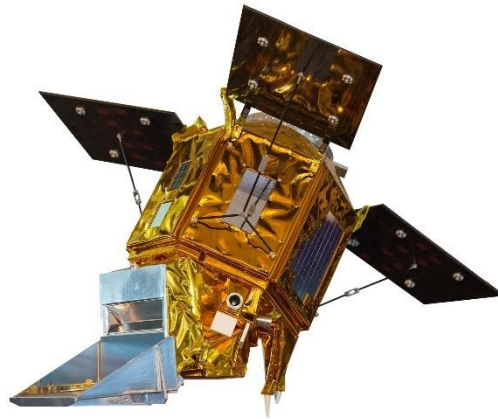
Figure 2-2. ESA Sentinel 5 Precursor satellite, rendered image [5].

The normalised Stokes vector components Q/I, U/I, and V/I can also be expressed in Poincaré sphere angles and degree of polarisation. This allows to potentially highlight differences between different space objects and orientations which may be less prominent in the spectrally resolved normalised Stokes vector.
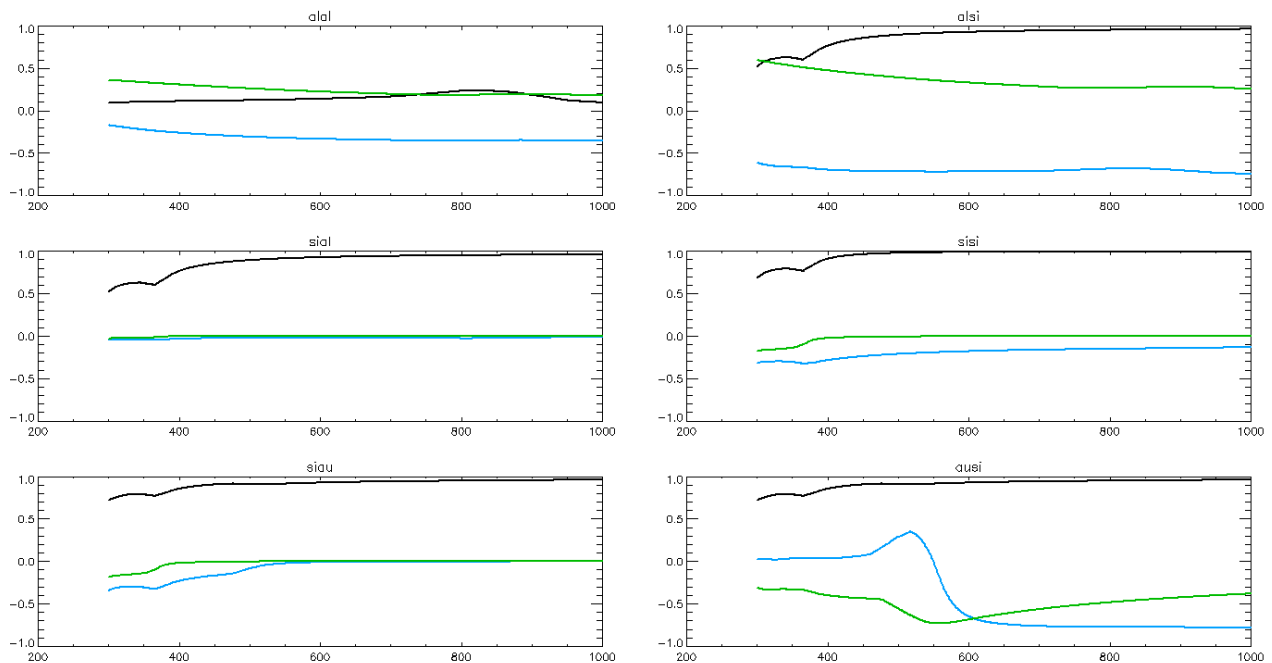

Figure 2-3. RMS variation of the Poincaré sphere angles in radians (blue and green curves) and the degree of polarisation (black curves) as function of wavelength in nm for 6 different material combinations: double scattering off aluminium and aluminium (alal), aluminium and silicon (alsi), silicon and aluminium (sial), silicon and silicon (sisi), silicon and gold (siau), and gold and silicon (ausi). Note the distinctly different spectral behaviour between the different material combinations but also order of scattering for the blue and green curves, representing the Poincaré sphere angles. There is much less distinction visible in the degree of polarisation (black curves)

Figure 2-1 is calculated for a scattering geometry that is beneficial for circular polarisation, in order to get an idea of the "typical" variation to expect in the Poincaré sphere angles assessed over all possible illumination geometries, the Stokes

vectors and Poincaré sphere angles were calculated for multiple material combinations and scattering geometries, which were subsequently used to determine the root mean square variation (RMS) over all geometries. Figure 2-3 shows the results of this calculation. It is clear from these plots that the RMS variation as function of wavelength of in particular the Poincaré sphere angles (green and blue curves) is very scattering material specific, allowing to distinguish between different materials just on the basis of spectrally resolved RMS variation of its polarisation features. This also implies that space objects composed of different materials or mixtures of materials may be distinguished.

Note that for a single observation point in the spectropolarimetric light curve of a space object the complete spectrally resolved and polarisation resolved information is available, and that as the space object progresses through its orbit, the scattering geometry and thus the spectropolarimetric signature changes. Figure 2-3 only gives a statistical summary of all possible scattering geometries, in reality a space object will pass through only a limited range of geometries and its individual spectropolarimetric light curve may be used for identification purposes of the object.

3. POLARISATION MODULATOR

The main part of the instrument is the modulator. This is composed of three prisms in Magnesium Fluoride, optically glued together (see Figure 3-1)[6][7][8]. In addition, the fast axis is differently oriented in each prism. Therefore, as can be observed in Figure 3-1, the prism (1), of apex angle ξ, has the fast axis oriented along the x-axis. The middle component of the modulator, (2), has the fast axis oriented along the z-axis. In the third wedge of apex angle ψ, the fast axis makes an angle of 45° with the x-axis, in the (xy)-plane.

The prismatic shape of the elements (1) and (3) ensures a continuous variation of the phase difference between the orthogonal components of light in the y direction.

Therefore, given the geometry and orientation of the fast axis, the first prism can convert any incoming state of polarisation, except the Q state, into a continuous variation of polarisation in the vertical direction.

The second prism, (2), plays only the role to keep everything together, into a single part. It helps also mitigate the deviation of rays, as it is built from the same material as the other two.

The last prism, (3), is complementary to the first one: it serves to modulate the Q state, left unaffected previously.

Using this geometry, the polarised light arriving collimated on the left side of the modulator exit the prisms exhibiting a continuous variation of the polarisation in the vertical direction. Therefore, by placing an analyser after this modulator, this variation can be converted into a variation in intensity, that can be measured with a detector, along the vertical direction.
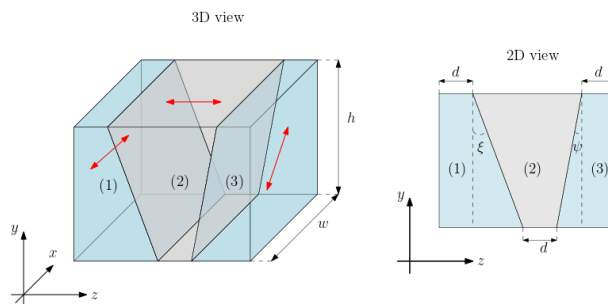

Figure 3-1. 3D and 2D view of the modulator. Each prism of the modulator has a particular orientation of the fast axis: along the x-axis in prism (1), along z in prism (2), and at 45° with respect to x-axis in the prism (3). The height of the modulator, h, must cover at least the largest period of the signal described by the Eq.(1). Because there is no modulation of the signal in the x direction, the width can be chosen according to the constraints of the optical system. Concerning the length, it is dictated by the height h, the angles ξ and ψ, and by the additional thickness, d.

To avoid the split of the ordinary and extraordinary rays and to decrease the frequencies of the modulation, the angles ξ and ψ must be kept as small as possible. Also, to aid manufacturing and handling of the optical component, an additional thickness, d, of constant value can be added to each prism.

Based on this architecture, the intensity of light detected after the passage through the modulator and the analyser follows the relation

$$I(\theta, y, \lambda) = \frac{1}{2}[S_1 + S_2 \cdot m(\theta, y, \lambda) + S_3 \cdot n(\theta, y, \lambda) + S_4 \cdot p(\theta, y, \lambda)] \tag{1}$$

where θ is the angle of the analyser with respect to the x-axis, y is the position in the vertical direction, λ is the wavelength, and $\vec{S} = [S_1, S_2, S_3, S_4]^T$ is the Stokes vector of the incoming light. The functions m, n, p, computed with the help of the Mueller calculus, are given by:

$$m(\theta, y, \lambda) = cos(2\theta)cos(\Delta\phi_3)$$
$$n(\theta, y, \lambda) = sin(2\theta)cos(\Delta\phi_1) + cos(2\theta)sin(\Delta\phi_1)sin(\Delta\phi_3) \tag{2}$$
$$p(\theta, y, \lambda) = sin(2\theta)sin(\Delta\phi_1) - cos(2\theta)cos(\Delta\phi_1)sin(\Delta\phi_3)$$

where $\Delta\phi_1$ and $\Delta\phi_3$ are the phase differences induced by the prisms (1) and (3):

$$\begin{cases} \Delta\phi_1 = \dfrac{2\pi}{\lambda}\Delta n(\lambda)[d + (h - y)tan(\xi)] \\ \Delta\phi_3 = \dfrac{2\pi}{\lambda}\Delta n(\lambda)[d + (h - y)tan(\psi)] \end{cases} \tag{3}$$

where $\Delta n(\lambda) = |n_o(\lambda) - n_e(\lambda)|$ is the absolute value of the difference between the ordinary and the extraordinary indices of refraction, also called the birefringence of the medium, while h is the height of the modulator.

From the Eq. (1) we infer that the intensity detected by the pixels in the y direction, when the wavelength is known and the orientation of the analyser θ well established, can be expressed by the following system:

$$\begin{pmatrix} I(y_1) \\ I(y_2) \\ \vdots \\ I(y_N) \end{pmatrix} = \frac{1}{2} \begin{pmatrix} 1 & m(y_1) & n(y_1) & p(y_1) \\ 1 & m(y_2) & n(y_2) & p(y_2) \\ \vdots & \cdot & \cdot & \cdot \\ 1 & m(y_N) & n(y_N) & p(y_N) \end{pmatrix} \begin{pmatrix} S_1 \\ S_2 \\ S_3 \\ S_4 \end{pmatrix} \tag{4}$$

Solving this system of equations for S_1, S_2, S_3, S_4 gives us access to the incoming state of polarisation.

The spectral limitation of this modulator is dictated by the transmission band and the birefringence of the material. With the help of Magnesium Fluoride, we can access the entire spectrum between 0.12 and 7 μm [6][7].
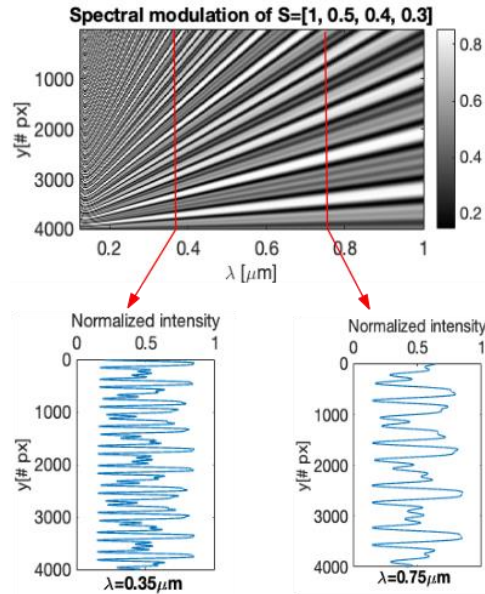
Figure 3-2. Spectral modulation of an incoming state of polarisation S=[1,0.5,0.4,0.3] obtained on a column of 4000 pixels, with a size of 5μm. In this simulation we supposed that the height of modulator is h=2cm, the apex angles are ξ=2.6°,ψ=1.8°, and the additional thickness is d=1mm. The orientation of the analyser was θ=72°.

Given the possibility to work at different wavelengths and the fact that the modulator is redundant in the x direction, then the x-axis can be used to spectrally disperse the light on the detector. Therefore, on the detector plane, we can have access simultaneously to the polarimetric information in the vertical direction, and to the spectral information in the horizontal.

For the manufacturing of the modulator, we have used the apex angles $\xi = 2.6°$ and $\psi = 1.8°$. Together with an orientation of the analyser at $\theta = 72°$, these values can ensure a hight efficiency of the modulation scheme of the polarimeter [9] and an almost equal precision on the measurement of the Stokes parameters. The additional thickness, d, is 1mm, ensuring easy and safe handling of the modulator.

4. BREADBOARD DESIGN

The breadboard optical design starts with the interface to the telescope focal plane. Input is considered to be a point source, limited in angular extent by the quality of the telescope and the seeing conditions of the atmosphere. An appropriately sized pinhole is placed around this point source. From this, a collimated beam is produced, followed by the polarisation modulator and analyser, and subsequently an equilateral prism to create the desired dispersion in the plane perpendicular to the polarisation modulation. A cylindrical lens images the pinhole in the spectral dimension onto the detector, while maintaining the polarisation modulation in the pupil plane of the instrument plus telescope. Figure 4-1 (left) shows an impression of the optical design, without the telescope which would be placed on the right.
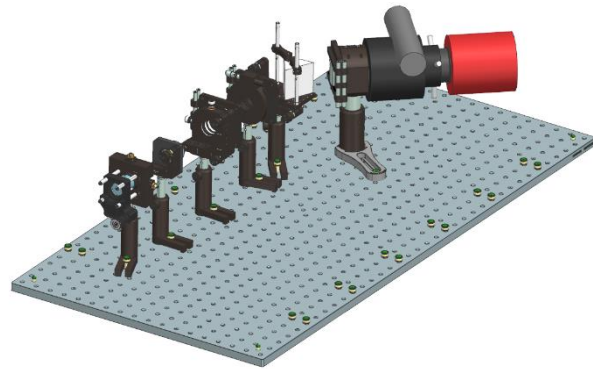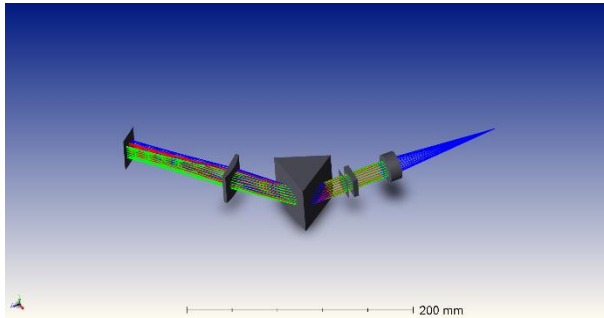
Figure 4-1. Left: Impression of the optical design of the spectropolarimeter. The incoming light is on the right, the detector on the left. Right: Rendered image of the optical and mechanical parts of the breadboard spectropolarimeter. Light enters on the left; the detector is mounted in the red cylinder on the right.

For laboratory use it is possible to place a microscope objective instead of a telescope in front of the pinhole. This allows characterisation of satellite mock-ups or flight spare models.

The optical and mechanical parts are all commercially off the shelf components, apart from the polarisation modulator. A rendered image of the breadboard spectropolarimeter (without the light tight enclosure) is shown in Figure 4-1 (right).

5. TEST BENCH DESIGN

The characterisation of the birefringent properties of the modulator is inspired by the one described by [10], and its implementation will be similar to the one presented in [11]. The purpose is to measure the phase birefringence ($\Delta\phi_1, \Delta\phi_3$) of the prisms and the fast axis orientation of the prisms constituting the modulator (α_1, α_3). The optical setup is presented in Figure 5-1.
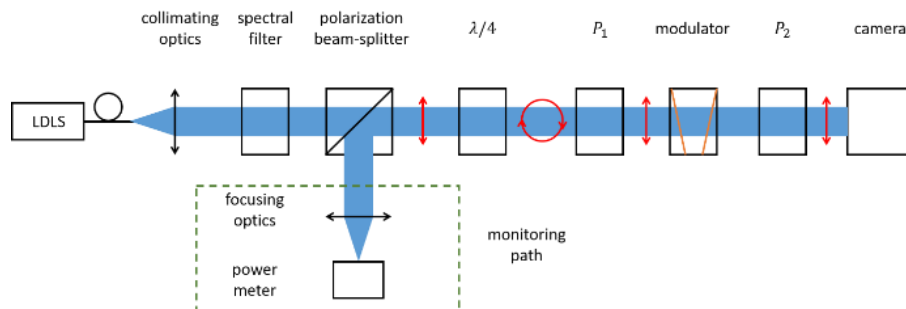

Figure 5-1. Scheme of the polarisation characterisation measurement setup, the beam is pictured in blue, the red arrows represent the polarisation at different places of the beam.

The setup is composed of:

- a fibered laser driven light source (LDLS), emitting light from 300 to 1500 nm,
- a spectral filter to define a small bandwidth for the measurement,
- collimating optics to convert the diverging beam at the end of the fibre into a collimated one,
- a polarisation beam-splitter, to provide a monitoring path and to define a reference polarisation
- a power meter for monitoring the power of the beam to correct for intensity variation during the acquisition
- a quarter wave-plate ($\lambda/4$) to create a circular polarisation,
- 2 linear polarisers on automated rotation stages (P_1 & P_2),
- the prism modulator,
- a CMOS camera.

The measurement principle is the following one. For a specific bandwidth, the transmission axis of P_1 will perform a full rotation by increments of $10°$. For each orientation of P_1 (θ), two maps of intensities will be recorded: $I_\parallel(x, y, \theta)$ & $I_\perp(x, y, \theta)$. $I_\parallel(x, y, \theta)$ corresponds to the intensity map recorded with the transmission axis of P_2 is parallel to the one of P_1 and $I_\perp(x, y, \theta)$ stands for the intensity when P_2 axis is perpendicular to P_1. Afterwards, the ratio of intensity Γ is computed as equation 1.

$$\Gamma(x, y, \theta) = \frac{I_\perp(x, y, \theta)}{I_\parallel(x, y, \theta)} \tag{5}$$

Using Mueller matrices for the polarisers and prisms, Γ can be expressed as a function of $\theta, \Delta\phi_1, \Delta\phi_3, \alpha_1$ & α_3. Then, by fitting this equation pixel by pixel, using θ as a variable, the values of the phase retardances and fast axis orientation can be computed (see Figure 5-2 for some curves of Γ for the wavelength of 633 nm for several heights in the modulator). Finally, those experimental values of the phase retardances and the fast axis orientations will be used as parameters for the measurement of the polarisation of incident beams during the real measurements.
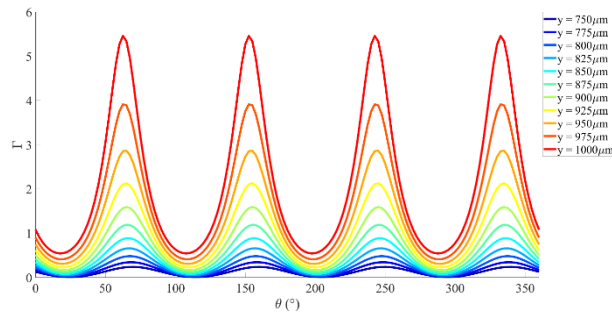

Figure 5-2. Representation of the intensities ratio Γ for pixels on the same column and at different height inside the modulator. The representation step was selected as 25μm to provide more variation with fewer curves. The real system will be on the 5μm range for the pixel size.

6. DATA ACQUISITION AND ANALYSIS PLANS

Once the spectropolarimeter breadboard is complete and the polarisation modulator has been characterised, the first step is to characterise the end-to-end performance of the breadboard with known polarisation sources. After that, the instrument will be equipped with a microscope objective in order to image a mock-up of a satellite onto the spectropolarimeter pinhole and simulate a point source observation. This will allow the first representative measurements with full control over the materials and the illumination-, scattering-, and viewing geometry.

The final test will be to mount the breadboard on a telescope with 800 mm diameter provided with a fast and accurate mount that was specified to track Low Earth Orbit satellites (Figure 6-1). Observations of sufficiently bright satellites (e.g. magnitude 9 and brighter) should yield sufficient quality measurements that allows in principle to reach normalised Stokes vector values to be assessed with about 0.001 precision or better, at the equivalent of 50 nm spectral resolution.
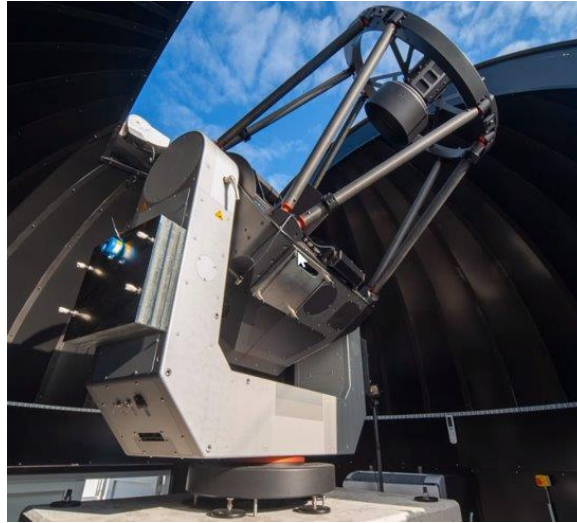
Figure 6-1. The 800 mm diameter telescope at TNO the Hague, to be used with the spectropolarimeter.

Data analysis will initially focus on understanding the measurement results, in particular the impact of the telescope and environmental parameters (temperature). As we expect from the telescope design that it will introduce complex instrumental polarisation [12], the data analysis will consider these instrument effects as well. A likely approach will be to analyse the measurements and express them not only in Stokes parameters $[S_1, S_2, S_3, S_4]^T$, but also express them in degree of total polarisation $p = \frac{1}{S_1}\sqrt{(S_2^2 + S_3^2 + S_4^2)}$, and angles χ and ψ on the Poincaré sphere, all as a function of wavelength.

As the different materials involved in scattering of sunlight at the satellite will affect the polarisation of the light, so will the mirrors in the telescope and the temperature effects of the polarisation modulator. The differences between the satellite and the instrument are that the reflection geometry and materials at the instrument side are well known, so any instrumental spectropolarimetric signatures can in principle be identified. This allows either correction of the signatures, or inclusion in an instrument model as known parameters that can thus separate the effects from the spectropolarimetric signatures of the incoming light.

A next layer of analysis could be interpretation of the spectropolarimetric results as visible fractions of materials at the satellite surface, similar to being done in [13], but in this case also using the polarimetric signature to help distinguish between different materials and even get an indication of multiple scattering.

The intention of these measurements and analyses is to investigate the potential of spectropolarimetry for space object identification and create a roadmap for further development.

7. SUMMARY AND DISCUSSION

We present our concept and breadboard design for a full Stokes spectropolarimeter intended for space object identification. The instrument concept allows measurement of point sources and separates the polarisation and spectral properties into two perpendicular dimensions on a 2-dimensional detector. Initial calculations suggest that geostationary satellites (typically with a brightness of stellar magnitude 9) could be measured with sufficient precision to allow useful investigations into means to further identify space objects. Brighter satellites can be measured with more ease, while fainter satellites could also be measured at the cost of temporal, spectral and polarisation resolution. Instrumental polarisation aspects are considered a challenge, but a methodology for a way forward to deal with this has been identified.

Currently, all hardware for the spectropolarimeter breadboard is in house and integration of the breadboard is foreseen to start this year, with first light intended to be obtained also this year.

The breadboard measurements will indicate whether the approach is sound, and in that case will allow detailing of a roadmap to arrive at a mature instrument and processing chain that can be used for Space Situational Awareness.

REFERENCES

[1] Ivan Ferrario, Eugenio Di Iorio, Fabrizio Silvestri, Ralph Snel, Quentin Chavet, Optical Technologies for Space Situational Awareness, 2nd ESA NEO and Debris Detection Conference, 2023

[2] R. Snel, B. Vasilescu, I. Ferrario, J. Loicq, P. Piron, E. Di Iorio, T. Hooftman, Q. Chavet, Full Stokes Spectropolarimetry for Space Object Identification, 2nd ESA NEO and Debris Detection Conference, 2023

[3] Endo, T., Ono, H., Hosokawa, M., et al. "Spectroscopic characterization of GEO satellites with Gunma LOW resolution Spectrograph" (2017), Advanced Maui Optical and Space Surveillance (AMOS) Technologies Conference, 2017amos.confE..81E

[4] Speicher, A., "Identification of Geostationary Satellites Using Polarization Data from Unresolved Images" (2015). Electronic Theses and Dissertations. 1050. https://digitalcommons.du.edu/etd/1050

[5] SkywalkerPL - Own work, CC BY 3.0, https://commons.wikimedia.org/w/index.php?curid=45634546

[6] B. Vasilescu, Y. Nazè, and J. Loicq, "Solution uniqueness and noise impact in a static spectropolarimeter based on birefringent prisms for full Stokes parameter retrieval," J. Astron. Telesc. Instrum. Syst. 6, 1 (2020).

[7] M.J. Dodge, "Refractive properties of magnesium fluoride",Appl.Opt.23,1980–1985(1984).

[8] H. H. Li, "Refractive index of alkaline earth halides and its wavelength and temperature derivatives", J. Phys. Chem. Ref. Data 9, 161–290 (1980).

[9] J. C. del Toro Iniesta and M. Collados, "Optimum modulation and demodulation matrices for solar polarimetry", Appl. Opt. 39, 1637 (2000)

[10] Emoto, A., Nishi, M., Okada, M., Manabe, S., Matsui, S., Kawatsuki, N., & Ono, H. (2010). Form birefringence in intrinsic birefringent media possessing a subwavelength structure. Applied optics, 49(23), 4355-4361.

[11] Piron, P., Catalan, E. V., Absil, O., & Karlsson, M. (2018). Birefringence measurements of diamond space-variant subwavelength gratings. Applied Optics, 57(17), 4909-4917.

[12] de Juan Ovelar, M., Snik, F., Keller, C. U. Venema, L., "Instrumental polarisation at the Nasmyth focus of the E-ELT", A&A, 562 (2014) A8, DOI: https://doi.org/10.1051/0004-6361/201321717

[13] Vasile, M. & Walker, L. & Dunphy, D. & Zabalza, J. & Murray, P. & Marshall, S. & Savitski, V. (2022). Intelligent Characterisation of Space Objects with Hyperspectral Imaging, Acta Astronautica, Volume 203, 2023, Pages 510-534, ISSN 0094-5765, https://doi.org/10.1016/j.actaastro.2022.11.039